Journal of Molecular Spectroscopy 348 (2018) 37–42

Contents lists available at ScienceDirect

Journal of Molecular Spectroscopy

journal homepage: www.elsevier.com/locate/jms

First analysis of the $\nu_3 + \nu_5$ combination band of SF_6 observed at Doppler-limited resolution and effective model for the $\nu_3 + \nu_5 - \nu_5$ hot band

M. Faye [a], L. Manceron [a,b,*], P. Roy [a], V. Boudon [c], M. Loëte [c]

[a] Synchrotron SOLEIL, AILES Beamline, L'Orme des Merisiers, Saint-Aubin F-91192, France
[b] Monaris, UMR 8233 CNRS-Université Pierre et Marie Curie, 4 Place Jussieu Case 49, 75252 Paris, France
[c] Laboratoire Interdisciplinaire Carnot de Bourgogne, UMR 6303 CNRS-Université de Bourgogne Franche-Comté, 9 avenue Alain Savary, BP 47870, F-21078 Dijon, France

ARTICLE INFO

Article history:
Received 17 August 2017
In revised form 4 January 2018
Accepted 9 January 2018
Available online 16 January 2018

ABSTRACT

Sulfur hexafluoride is a greenhouse gas with a long lifetime in the atmosphere and an important tracer for air mass circulation atmospheric models. The IR spectrum of this heavy species, however, features many hot bands at room temperature (at which only 30% of the molecules lie in the ground vibrational state), especially those originating from the lowest, ν_6 and $\nu_5 = 1$ vibrational states. Using a cryogenic long path cell with variable optical path length and temperatures regulated between 168 and 163 K, coupled to Synchrotron Radiation and a high resolution interferometer, Doppler-limited spectra of the very weak $\nu_3 + \nu_5$ band near 1450 cm^{-1} have been recorded. Low temperature was used to limit the presence of hot bands and simplify the rotational structure. The spectrum has been analyzed thanks to the XTDS software package. Combining with the results obtained previously on the weak difference bands in the far infrared region involving the $\nu_5 = 1$ states, we are thus able to use the tensorial model to propose a spectroscopic parameter set for modelling the strong $\nu_3 + \nu_5 - \nu_5$ hot band. The model constitutes a coherent set of molecular parameters and enable spectral simulation for atmospheric sounding. Test simulations at different temperatures and in nitrogen broadened conditions are presented and compared with new experimental cross section data for the absorption region relevant for atmospheric quantification.

© 2018 Elsevier Inc. All rights reserved.

1. Introduction

Sulfur hexafluoride (SF_6), an octahedral molecule of O_h symmetry, is of interest in atmospheric chemistry as a potent greenhouse gas, even if present at part-per-trillion scale. Its steady growth caused it to be listed in the Kyoto protocol among the atmospheric gases to be monitored [1,2]. Because of its very long lifetime in the atmosphere (about 3200 years) it is also used to assess the so-called "mean age" of stratospheric air and used to check the currently accepted air circulation models [3–4]. In particular, its strong infrared absorption near 10 μm is used to monitor its presence in the atmosphere from ground-based stations [5], aircrafts [6] or satellites [7–9].

The infrared spectrum of gaseous SF_6 has been extensively studied at low resolution (see [10] and therein) and all its fundamentals have been observed at high to very high resolution and analyzed in detail [11–18].

The six fundamentals of SF_6 are three stretching motions, ν_1 to ν_3, of A_{1g}, E_g and F_{1u} symmetries and three bending modes, ν_4 to ν_6, of F_{1u}, F_{2g} and F_{2u} symmetries. Only ν_3 (near 948 cm^{-1}, $I_{\nu_3} \simeq 1130$ km/mole) and ν_4 (near 615 cm^{-1}, $I_{\nu_4} \simeq 70$ km/mole) are infrared active and strongly absorbing. Thus, the ν_3 region, falling in the 8—12 μm atmospheric thermal IR window is obviously the best choice for *in situ* SF_6 quantification [7,8]. Of course, concentration retrieval is normally based on molecular line databases [5,19] but for SF_6, as pointed out in by several workers [5,18], these databases are far too incomplete. This is due to the fact that, even if the ν_3 mode is well known, it is strongly overlapped by many hot bands originating from a variety of populated vibrational levels (about 32% population in the ground state at 293 K), from which only a few have been rigorously modelled [20]. To alleviate this difficulty, some workers have used an effective "pseudo-line list" approach [5], elaborated on a series of cross section measurements at moderate spectral resolution and four temperatures between 216 and 295 K by Varanasi et al. [21]. In order to improve or, at least, validate this approach, it seems desirable to find a way to determine sets of spectroscopic parameters enabling a rigorous modelling of the hot bands array in the ν_3 region. Following our previous study

* Corresponding author.
E-mail address: laurent.manceron@synchrotron-soleil.fr (L. Manceron).

https://doi.org/10.1016/j.jms.2018.01.004
0022-2852/© 2018 Elsevier Inc. All rights reserved.

on the weak $\nu_1+\nu_3-\nu_1$ and $\nu_2+\nu_3-\nu_2$, we pursue our strategy, finding difference or combination bands in isolated spectral ranges to model properly either the initial or final vibrational levels of the transitions. In a previous, recent study, we have observed the $\nu_2+\nu_4-\nu_5$ band to determine an improved spectroscopic parameter set for the $\nu_5=1$ state [22], using the newly developed instrumentation at Synchrotron SOLEIL (France), involving synchrotron radiation [24,25], a cryogenic long path cell [26] and high sensitivity detectors [27]. Next, this band has been analyzed using the HTDS module for spherical top molecules of the XTDS software [28,29] based on the tensorial formalism developed in the Dijon group for such highly symmetrical molecules.

To model the corresponding, $\nu_3+\nu_5-\nu_5$ hot band, a similar effort is needed on the upper, $\nu_3=\nu_5=1$ state. Fortunately, given the usual symmetry considerations ($F_{1u}\otimes F_{2g}=A_{2u}\oplus E_u\oplus F_{1u}\oplus F_{2u}$), the $\nu_3+\nu_5$ combination level contains one IR-active component and is, in principle, directly accessible in absorption. Practically, it is a very weak band, which has puzzled experienced spectroscopists in the past. At room temperature, it appears as a broad, structureless band peaking at about 1456 cm^{-1}, which is far below the position expectable from the wavenumbers of ν_3 and ν_5 ($\simeq$948 + 523 = 1471 cm^{-1}). In their comprehensive study of more than twenty-nine bands of SF_6 [30] to develop a coherent picture of anharmonic effects, McDowell and Krohn wrote at the time: "No Q branch is evident near the band center calculated near 1470 cm^{-1} or elsewhere, and no analysis was possible. This fuzzball of a band remains the most puzzling of all SF_6 IR absorptions.".

In the course of our investigations, we could acquire new data at much improved resolution and low temperature, which revealed more details. This study presents these results, along with an analysis of the $\nu_3+\nu_5$ combination band, a determination of the $\nu_3=\nu_5=1$ state parameters using the Dijon tensorial formalism and software, and predictions of the $\nu_3+\nu_5-\nu_5$ hot band which are compared with new cross section data obtained here in the ν_3 region.

2. Experimental results

Because of the weakness of the combination band, a long optical path length at low temperature was required. Several high resolution spectra were recorded on the AILES Beamline at Synchrotron SOLEIL on the Synchrotron light source coupled to the Bruker 125HR interferometer [24,25] using the cryogenic long path cell regulated at 168 K temperature along the entire optical path. This setup has been fully described elsewhere [26]. SR radiation was used as a source with 450 mA ring current in the multi bunch mode. A spectrum with a gas pressure of 2.4 mbar of SF_6 (Air Liquide, France, 99.99% purity) was recorded at 0.001 cm^{-1} resolution, with no apodization (Boxcar option), 5.06 cm/s scanner velocity using a Ge/KBr beamsplitter and a 4 K-cooled home-made HgCdTe photoconductor with a cold, 1180—1800 cm^{-1} band pass filter [27]. 320 interferograms were averaged in a total recording time of about 16 h and processed against a background of the empty cell taken at the same temperature at 0.01 cm^{-1} resolution. The path length was set to 141 m. For these measurements, the cell outer windows were switched from diamond to AR-coated ZnSe, improving the optical throughput by a factor of 1.9. Spectra were zero-filled, corrected for channelling effects and calibrated using well-known water and carbon dioxide or carbonyl sulphide rotational lines [28]. A series of spectra at high (0.001 cm^{-1}) to low (0.1 cm^{-1}) resolution was acquired at variable temperatures using a different set-up. For absorption cross section measurements, a short optical path stainless steel absorption cell with wedged diamond windows, which could be cooled by a flow of cold nitrogen gas down to 130 K was fitted directly in the spectrometer sample compartment. For these measurements, SF_6/N_2 mixtures with fixed and precisely known pressure ratios of 0.5–1% were prepared in advance, using 1 mbar and 1000 mbars range temperature-controlled capacitive gauge and a 3-l stainless steel tank. After equilibration overnight, a known pressure between 3 and 20 mbars was introduced in the cell and, when desired, completed by a precise amount of pure nitrogen as a broadening gas.

3. Theoretical model

The theoretical model used here is based on the cubic tensor formalism and the vibrational extrapolation developed by the Dijon group [29,31,32]. We simply recall the principles here; the reader should refer to the previous references for more detail about the notations. In the general case, vibrational levels are grouped in series of polyads called P_k with $k=0,\ldots,n$. For $k=0$, we have P_0 which is the ground state (GS). In the particular case of SF_6, where no clear resonance has been evidenced, the P_k terms designate here single vibrational states, which enables us to build up a model treating effectively the band as isolated, while transferring previously acquired knowledge on the intermediate levels. The Hamiltonian operator is thus written as follow:

$$\mathcal{H}=\mathcal{H}_{\{P_0\equiv GS\}}+\mathcal{H}_{\{P_1\}}+\ldots+\mathcal{H}_{\{P_k\}}+\ldots+\mathcal{H}_{\{P_{n-1}\}}+\mathcal{H}_{\{P_n\}}. \tag{1}$$

where the different $\mathcal{H}_{\{P_k\}}$ terms which contain the rovibrational operators are expressed in the following form:

$$\mathcal{H}_{\{P_k\}}=\sum_{\text{all indexes}} t^{\Omega(K,n\Gamma)\Gamma_v\Gamma'_v}_{\{s\}\{s'\}}\beta\left[{}^{\varepsilon}V^{\Omega_v(\Gamma_v\Gamma'_v)\Gamma}_{\{s\}\{s'\}}\otimes \mathrm{R}^{\Omega(K,n\Gamma)}\right]^{(A_{1g})}. \tag{2}$$

In this Eq. (2), the $t^{\Omega(K,n\Gamma)\Gamma v\Gamma' v}_{\{s\}\{s'\}}$ are the parameters to be determined, while ${}^{\varepsilon}V^{\Omega_v(\Gamma_v\Gamma'_v)\Gamma}_{\{s\}\{s'\}}$ and $\mathrm{R}^{\Omega(K,n\Gamma)}$ are vibrational and rotational operators, respectively, and of respective degree Ω_v (in normal mode creation and annihilation operators) and Ω (in angular momentum componants, J_x, J_y or J_z). β is a factor that allows the scalar terms ($\Gamma=A_{1g}$) to match the usual terms like B_0J^2, *etc.* and $\otimes$ represents the tensorial product. To generalize, we have:

$$\beta=\begin{cases}\sqrt{[\Gamma_v]}\left(\sqrt{3}/4\right)^{\Omega/2}, & \text{if}(K,n\Gamma)=(0,0A_{1g}),\\ 1, & \text{otherwise.}\end{cases} \tag{3}$$

The order of each individual term is defined as $\Omega+\Omega_v-2$.

In this model we deal with an effective Hamiltonian which is obtained, for a given polyad P_k, by the projection of H in the P_n Hilbert subspace; see Eq. (4).

$$\begin{aligned}H^{\langle P_n\rangle}&=P^{\langle P_n\rangle}\mathcal{H}P^{\langle P_n\rangle}\\&=H^{\langle P_n\rangle}_{\{\mathrm{GS}\}}+H^{\langle P_n\rangle}_{\{P_1\}}+\ldots+H^{\langle P_n\rangle}_{\{P_k\}}+\ldots+H^{\langle P_n\rangle}_{\{P_{n-1}\}}+H^{\langle P_n\rangle}_{\{P_n\}}.\end{aligned} \tag{4}$$

This Hamiltonian expression allows the systematic treatment of any polyad system.

The calculation of the effective Hamiltonian matrix was performed in the coupled rovibrational basis

$$\left|\left[\Psi^{(C_v)}_{v}\otimes\Psi^{(J,nC_r)}_{r}\right]^{(C)}\right\rangle, \tag{5}$$

where $\Psi^{(J,nC_r)}_r$ is a rotational wavefunction with angular momentum J, rotational symmetry species C_r and multiplicity index n and C the overall symmetry species ($C=C_v\otimes C_r$). The effective dipole moment operator, used to calculate transition intensities is expanded in a similar way. It is expanded here up to order 2 (see below) and its matrix elements are calculated in the Hamiltonian's eigenbasis set.

4. Analysis

As mentioned above, the $\nu_3 + \nu_5$ band has so far been presented as one of the most enigmatic SF_6 bands. Low resolution studies [30,33] indicate that the most intense peak is observed around 1456 cm^{-1}. This positioning of the band center is abnormally distant from the supposed theoretical position which should be around 1470 cm^{-1}, near to 1472.1 cm^{-1}, the sum of the band centers of ν_3 and ν_5.

In a first assumption, it was supposed that this cluster of transitions towards 1456 cm^{-1} would possibly be due to hot bands. The idea was to record a spectrum at a temperature low enough to have mainly the cold band, $\nu_3 + \nu_5$.

In order to clearly distinguish the rotational structure, we recorded the $\nu_3 + \nu_5$ band at 10^{-3} cm^{-1} resolution with a sample at 2.4 mbar pressure, to avoid pressure broadening. The long optical path length makes it possible to compensate for the low pressure and obtain a satisfactory absorption. Under these conditions, we could there obtain a spectrum showing a clear $P\,Q\,R$ structure with the Q branch occurring as expected around 1470 cm^{-1} (see Fig. 1). However, the most intense part that was supposed to be due to the hot band persists even at 168 K. We could so conclude that these transitions are therefore lines of the P branch of $\nu_3 + \nu_5$, with an unusually strong intensity (see discussion below).

We perform our analysis by using the tensorial formalism with the HTDS package of the XTDS software. The effective hamiltonian corresponding to the $\nu_3 + \nu_5$ combination band is written as Eq. (6),

$$H^{\langle \nu_3+\nu_5\rangle} = P^{\langle \nu_3+\nu_5\rangle}\mathcal{H}P^{\langle \nu_3+\nu_5\rangle} = H^{\langle \nu_3+\nu_5\rangle}_{\{P_0=GS\}} + H^{\langle \nu_3+\nu_5\rangle}_{\{P_1\}} + H^{\langle \nu_3+\nu_5\rangle}_{\{P_2\}} + H^{\langle \nu_3+\nu_5\rangle}_{\{P_3\}}. \quad (6)$$

This effective Hamiltonian is developed to the 6^{th} order and the upper J quantum number value is set to 110 to simulate the experimental spectrum. As mention in the introduction, the $\nu_3 + \nu_5$ band shows four sub-levels, since $F_{1u} \otimes F_{2g} = A_{2u} \oplus E_u \oplus F_{1u} \oplus F_{2u}$.

A correct positioning of each sub-level is required to reproduce the experimental spectrum. We based our starting point on the estimates of the anharmonic vibrational constants $X_{35}, G_{35}, T_{35}, S_{35}$ resulting from the anharmonic force field determined by Heenan [34]. The latter determined values for these parameters (X_{35} = −0.850 cm^{-1}, G_{35} = 0.242 cm^{-1}, T_{35} = 0.245 cm^{-1}, S_{35} = −0.04 cm^{-1}), after semi-empirical adjustment on the band centers as were supposed to be known in the 1980s [35]. Even if these values were obtained from calculations based on the approximative position of the band centers, they allow us to approach the positions of the four sub-levels, in the first guess. Moreover, we proceeded from the hypothesis that only the F_{1u} sub-level (having the symmetry which confers directly an infrared activity) will have a predominant component of the dipole moment. Secondly, the higher-order parameters of the dipole moment have been optimized and, by a patient and systematic variation of the positions of the sub-levels, we have tried to reproduce as best as possible the shape of the spectrum until the first assignments were possible (see Fig. 2). Fig. 2 illustrates the main points but calls for a few comments. With a single, zeroth order F_{1u} component, the band would have a symmetrical, P, Q, R structure (sketch a, top), while adding a first-order F_{1u} component helps greatly in reproducing the strong intensity of the P branch but does not reproduce many weaker lines in the P and R branch wings. (sketch b, middle). Finally, adding a ten times weaker F_{2u} component is an effective way of spreading the intensity to other, weaker lines observed in the spectrum and not reproducible with a single dipole moment component hamiltonian (sketch c, bottom). Table 1 gives the dipole moment values adjusted manually to the experimental spectrum.

For instance note that the set of weak lines observed above 1476 cm^{-1} belong to the E_u symmetry component manifold, weakly coupled to the other components and thus IR activated. The physical causes behind these effects will be discussed in Section 5.

Then, an adjustment of the parameters (positions of the sub-levels, variation of the rotational and distortion constants) allowed us to improve the prediction and make new assignments. This cycle was repeated until no improvement could be made. With 23 effective hamiltonian parameters, we assigned and fitted 700 lines with a J_{max} value of 90 and a standard deviation of 1.23 × $10^{-3}$$cm^{-1}$. We present in Table 2 the parameters optimized for the level $v_3 = v_5 = 1$ and its four subcomponents and the result of the simulation is compared in Fig. 3 to the experiment. Fig. 4 shows the details in the P branch of the $\nu_3 + \nu_5$ band.

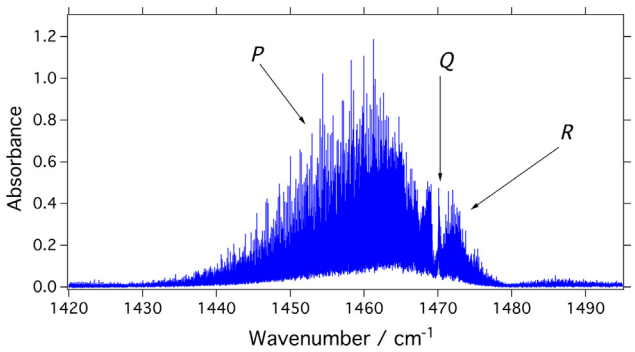

Fig. 1. The $\nu_3 + \nu_5$ band measured at 10^{-3} cm^{-1} resolution, 168 K temperature, 2.4 mbar pressure and 141 m path length.

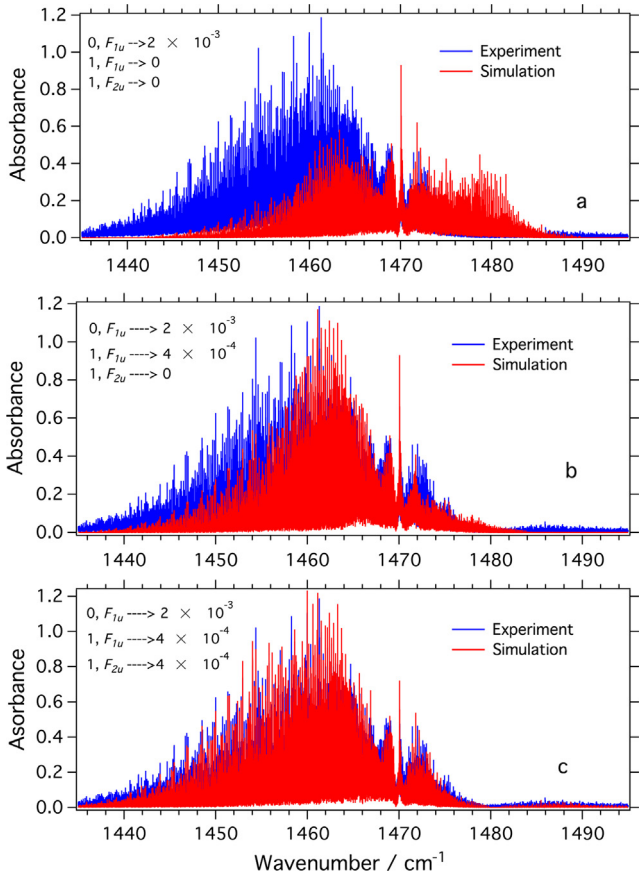

Fig. 2. Relative line intensities variation depending on the values of the dipole moment components parameters (in Debye).

Table 1
Effective dipole moment parameters values the $\nu_3 + \nu_5$ band.

$v = 0 \rightarrow \nu_{3,5} = 1$	$\Omega(K, n\Gamma)$	$\{s\}$	$\{s'\}$	Value/D
	$0(0,0A_{1g})$	$000000A_{1g}$	$001010F_{1u}$	2×10^{-3}
	$1(1,0F_{1g})$	$000000A_{1g}$	$001010F_{1u}$	4.42×10^{-4}
	$1(1,0F_{1g})$	$000000A_{1g}$	$001010F_{2u}$	4.42×10^{-4}

Table 2
Effective Hamiltonian parameters of the $\nu_3 + \nu_5$ combination band. Ground state, $\nu_5 = 1$ and $\nu_3 = 1$ parameters are taken from Refs. [22,23], respectively.

Ordre	$\Omega\ (K, n\Gamma)$	Parameters		Values/cm^{-1} (St.Dev)	Usual notations
		$\{s\}$	$\{s'\}$		
2	$0(0,0A_{1g})$	$001010A_{2u}$	001010_{A2u}	$-6.605(85) \times 10^{-1}$	A_{2u} sublevel
4	$2(0,0A_{1g})$	$001010A_{2u}$	$001010A_{2u}$	$3.09(14) \times 10^{-4}$	
3	$1(1,0F_{1g})$	$001010A_{2u}$	$001010F_{2u}$	$3.59(17) \times 10^{-3}$	$A_{2u} - F_{2u}$ interaction
2	$0(0,0A_{1g})$	$001010E_u$	$001010E_u$	$7.557(36) \times 10^{-1}$	E_u sublevel
4	$2(0,0A_{1g})$	$001010E_u$	$001010E_u$	$1.025(24) \times 10^{-4}$	
3	$1(1,0F_{1g})$	$001010E_u$	$001010F_{1u}$	$-4.884(83) \times 10^{-3}$	$E_u - F_{1u}$ interaction
3	$1(1,0F_{1g})$	$001010E_u$	$001010F_{2u}$	$1.10(77) \times 10^{-4}$	$E_u - F_{2u}$ interaction
2	$0(0,0A_{1g})$	$001010F_{1u}$	$001010F_{1u}$	$-2.54006(71)$	F_{1u} sublevel
3	$1(1,0F_{1g})$	$001010F_{1u}$	$001010F_{1u}$	$4.885(52) \times 10^{-3}$	
4	$2(0,0A_{1g})$	$001010F_{1u}$	$001010F_{1u}$	$4.62(12) \times 10^{-5}$	
4	$2(2,0E_g)$	$001010F_{1u}$	$001010F_{1u}$	$-1.868(44) \times 10^{-5}$	
4	$2(2,0F_{2g})$	$001010F_{1u}$	$001010F_{1u}$	$1.38(13) \times 10^{-5}$	
5	$3(1,0F_{1g})$	$001010F_{1u}$	$001010F_{1u}$	$-2.18(15) \times 10^{-7}$	
5	$3(3,0F_{1g})$	$001010F_{1u}$	$001010F_{1u}$	$9.5(2.6) \times 10^{-8}$	
3	$1(1,0F_{1g})$	$001010F_{1u}$	$001010F_{2u}$	$-1.678(30) \times 10^{-3}$	$F_{1u} - F_{2u}$ interaction
4	$2(2,0E_g)$	$001010F_{1u}$	$001010F_{2u}$	$-5.73(28) \times 10^{-6}$	
2	$0(0,0A_{1g})$	$001010F_{2u}$	$001010F_{2u}$	$-2.85614(93)$	F_{2u} sublevel
3	$1(1,0F_{1g})$	$001010F_{2u}$	$001010F_{2u}$	$-8.425(44) \times 10^{-3}$	
4	$2(0,0A_{1g})$	$001010F_{2u}$	$001010F_{2u}$	$9.30(23) \times 10^{-5}$	
4	$2(2,0E_g)$	$001010F_{2u}$	$001010F_{2u}$	$4.47(46) \times 10^{-5}$	
4	$2(2,0F_{2g})$	$001010F_{2u}$	$001010F_{2u}$	$9.15(57) \times 10^{-5}$	
5	$3(1,0F_{1g})$	$001010F_{2u}$	$001010F_{2u}$	$4.94(14) \times 10^{-7}$	
5	$3(3,0F_{1g})$	$001010F_{2u}$	$001010F_{2u}$	$-2.28(18) \times 10^{-7}$	

The positions of the four vibrational subcomponents are sketched on the simulation Fig. 3. Note that the positions and even the ordering for the A_{2u}, E_u, F_{1u} and F_{2u} levels differ slightly from those predicted from the empirical anharmonic force field of Heenan (1476.328 cm^{-1}, 1473.853 cm^{-1}, 1473.825 cm^{-1} and 1474.474 cm^{-1} for the A_{2u}, E_u, F_{1u} and F_{2u} levels, respectively).

5. Discussion on the band intensity

It is quite difficult at this stage to perform theoretical predictions for this band. But we can give hints about the origin of the observed anomalous band profile (*i.e.* the origin of effective dipole moment parameters from Table 1) and what data would be needed to perform quantitative calculations.

We consider here all SF_6 bands as isolated. But, of course, many interactions between them do exist and, even if they are small, they can induce intensity perturbations. Neglecting interactions in the Hamiltonian implies performing a perturbation calculation. This is usually done as a contact transformation in the form defined by Van Vleck [31,36]. If we can write the molecular rovibrational Hamiltonian and dipole moment operators as the following expansions:

$$H = H_0 + \lambda H_1 + \lambda^2 H_2 + \ldots \tag{7}$$

$$\mu_\alpha = \mu_{0\alpha} + \lambda \mu_{1\alpha} + \lambda^2 \mu_{2\alpha} + \ldots \tag{8}$$

where $\lambda = 1$ is used to indicate the development order and $\alpha = x, y$ or z, then the transformed effective Hamiltonian is written as the sum of the following terms:

$$\widetilde{H}_0 = H_0, \tag{9}$$

$$\widetilde{H}_1 = H_1 + i[S_1, H_0], \tag{10}$$

$$\widetilde{H}_2 = H_2 + i[S_1, H_1] - \frac{1}{2}[S_1, [S_1, H_0]] + i[S_2, H_0], \tag{11}$$

where S_1 and S_2 are the generators of the transformation. They are rovibrational operators defined by the above formulas so that $\widetilde{H}_1$ and $\widetilde{H}_2$ are diagonal in their vibrational part. In the present case, if we wish to isolate the $\nu_3 + \nu_5$ band, one can show that S_1 contains Coriolis rovibrational interactions between the $\nu_3 = 1, \nu_4 = 1$ and $\nu_6 = 1$ vibrational states, as well as Fermi vibrational interactions between the same three states and $\nu_3 = \nu_5 = 1$. S_2 contains so-called Darling-Dennison rovibrational interactions between $\nu_3 = 1$ or $\nu_4 = 1$ and $\nu_3 = \nu_5 = 1$. It should be noticed that not interaction with the $\nu_5 = 1$ vibrational state is implied here, due to its g parity (while the other states mentioned here have u parity); in centrosymmetric molecules like SF_6 there are no rovibrational interactions between states of opposite parity. We used the effective Hamiltonian described in the previous Section and fitted the experimental assignments, implicitly including these interactions (they implicitly contribute to the fitted parameters). But, at present, they are not known individually and it is thus not possible to theoretically predict the corresponding effective Hamiltonian parameters.

Once the contact transformation is determined in this way, it should be applied to the effective dipole moment operator, in order to calculate correct line intensities. This operator has the following form:

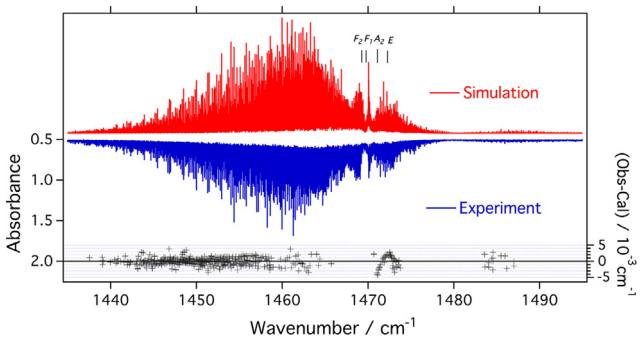

Fig. 3. The $\nu_3 + \nu_5$ band recorded at low temperature (168 K, with 141 m path and 2.4 mb SF_6 pressure, compared to simulation), with the long path cell. In blue (lower trace) the experimental spectrum. In red (upper trace) the simulated spectrum with the parameters of Table 2. Middle part fit residuals (10^{-3} cm^{-1}). (For interpretation of the references to colour in this figure legend, the reader is referred to the web version of this article.)

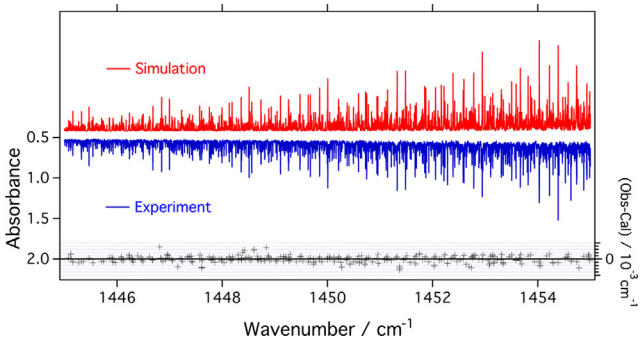

Fig. 4. Details in the *P* branch of the band.

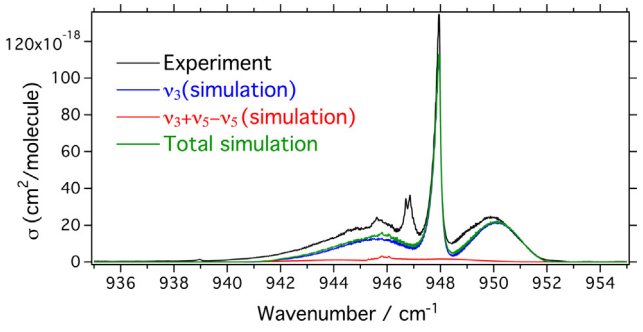

Fig. 5. Global view of the ν_3 region. The upper curve (black) represents the experimental cross section at 213 K. In blue and red, simulations for the ν_3 and $\nu_3 + \nu_5 - \nu_5$ bands. In green, the sum of the two contributions. (For interpretation of the references to colour in this figure legend, the reader is referred to the web version of this article.)

$$\widetilde{\mu}_{0\alpha} = \mu_{0\alpha}, \tag{12}$$

$$\widetilde{\mu}_{1\alpha} = \mu_{1\alpha} + i[S_1, \mu_{0\alpha}], \tag{13}$$

$$\widetilde{\mu}_{2\alpha} = \mu_{2\alpha} + i[S_1, \mu_{1\alpha}] - \frac{1}{2}[S_1, [S_1, \mu_{0\alpha}]] + i[S_2, \mu_{0\alpha}]. \tag{14}$$

When applying this, one can show that $\widetilde{\mu}_{1\alpha}$ contains contributions of the form:

$$\left[-V^{3(F_{1u}F_{1u})A_{1g}}_{\{s\}\{35\}}, +V^{3(A_{1g}F_{1u})F_{1u}}_{\{0\}\{s\}} \right] \rightarrow V^{3(A_{1g}F_{1u})F_{1u}}_{\{0\}\{35\}}, \tag{15}$$

with $s = 3$ or 4, and corresponds to the first (main) parameter in Table 1. Here, $[\ldots,\ldots]$ is a commutator and the arrow ($\rightarrow$) means "contributes to". Then, $\widetilde{\mu}_{2\alpha}$ contains:

$$\left[\left(+V^{2(F_{1u}F_{1u})F_{1g}}_{\{3\}\{4\}} \otimes R^{1(1,F_{1g})} \right)^{(A_{1g})}, +V^{3(A_{1g}F_{1u})F_{1u}}_{\{0\}\{45\}} \right] \rightarrow \left(-V^{3(A_{1g}C_u)C_u}_{\{0\}\{35\}} \otimes R^{1(1,F_{1g})} \right)^{(F_{1u})}, \tag{16}$$

and

$$\left[\left(+V^{2(F_{1u}F_{1u})F_{1g}}_{\{3\}\{6\}} \otimes R^{1(1,F_{1g})} \right)^{(A_{1g})}, +V^{3(A_{1g}F_{1u})F_{1u}}_{\{0\}\{56\}} \right] \rightarrow \left(-V^{3(A_{1g}C_u)C_u}_{\{0\}\{35\}} \otimes R^{1(1,F_{1g})} \right)^{(F_{1u})}, \tag{17}$$

where $C_u = F_{1u}$ or F_{2u}, corresponding to the second and third parameters in Table 1. Two rovibrational contributions, due to Coriolis and Darling-Dennison interactions, are responsible for the unusual band profile that we observe. As already mentioned, a quantitative estimation of the effective dipole moment parameters associated to these parameters is not yet possible, because of the lack of data concerning the implied interactions, but the present qualitative description shows at least which contributions could explain the above-determined intensity contributions.

6. Relation to atmospheric measurements

From the analysis of $\nu_3 + \nu_5$ band, we have obtained a parameter set for the $v_3 = v_5 = 1$ level and, from the study of $\nu_2 + \nu_4 - \nu_5$ [22], we had previously obtained parameters of $v_5 = 1$. It is now possible to carry out an exact simulation of the hot band $\nu_3 + \nu_5 - \nu_5$ in any conditions relevant to atmospheric studies. As an example, we have chosen the conditions for observation in the upper troposphere (about 12 km). We have therefore been able to compare an adequate simulation with the experimental spectrum recorded at 0.01 cm^{-1} resolution obtained by diluting 1.28×10^{-1} mbar of SF_6 for 200 mbar of nitrogen at 213 K temperature in a 5.1 cm cell see Fig. 5. To simulate these bands (the ν_3 fundamental and the $\nu_3 + \nu_5 - \nu_5$ hot band), we assume that the $\nu_3 + \nu_5 - \nu_5$ hot band has the same dipole moment value as the ν_3 fundamental. The intensity of each hot band is then normalized to the population of its lower level. The pressure broadening is obtained by taking γ_{N_2} = 0.09 cm^{-1}/ atm. This value of γ_{N_2} has also been determined in a systematic temperature study led in this laboratory. These conditions correspond to those of the upper troposphere. Under these conditions, the contribution of this hot band is minor, mainly seen on the wing of the absorption near 945.5 cm^{-1}, which must be due to another hot band. The most likely contributions, following the $\nu_3 + \nu_6 - \nu_6$ near 945.8 cm^{-1} are $\nu_3 + \nu_4 - \nu_4$ and, next, $\nu_3 + 2\nu_6 - 2\nu_6$.

7. Conclusion

By using the synchrotron radiation combined with a set of tools such as the HR-FTIR Bruker spectrometer and our cryogenic long path cell and high sensitivity detector, we recorded the $\nu_3 + \nu_5$ band of SF_6. We have then used the HTDS package of the XTDS program to simulate the spectrum and fit the hamiltonian parameters of the $v_3 = v_5 = 1$ level. We could thus solve the mystery of the very unusual shape of the band; we could show that is does posses an Q branch ate 1470 cm^{-1}, as expected, and that its shape is due to an abnormal intensity distribution, leading to a very prominent *P* branch. This is due to yet undetermined interactions for which we could give some theoretical hints, although a detailed explanation will require more investigations. Combining this knowledge with the previous improved set of parameters obtained for the $v_5 = 1$ level, a rigorous modeling of the $\nu_3 + \nu_5 - \nu_5$ hot band becomes possible. A comparison with low temperature cross section in conditions corresponding to the upper troposphere is presented here and the contribution of this hot band clearly

explicited. Work is in progress using comparable strategies to elucidate the other main hot bands.

Acknowlegements

We gratefully acknowledge support from the DIM-Analytics program of the Ile de France Region and SOLEIL, as well as the LEFE-CHAT program of CNRS.

References

[1] M. Khalil, Annu. Rev. Energy Environ. 24 (1999) 645.
[2] T. Reddmann, R. Ruhnke, W. Kouker, J. Geophys. Res. 106 (2001) 14525.
[3] M. Diallo, B. Legras, A. Chédin, Atmos. Chem. Phys. 12 (2012) 12133.
[4] J. Reilly, M. Mayer, J. Harnisch, Environ. Model. Assess 7 (2002) 217.
[5] J. Krieg, J. Nothholt, E. Mahieu, C.P. Rinsland, R. Zander, J. Quant. Spectrosc. Radiat. Trans. 92 (2005) 383.
[6] A.E. Andrews, K.A. Boering, B.C. Daube, S.C. Wofsy, M. Loewenstein, H. Jost, J.R. Podolske, C.R. Webster, R.L. Herman, D.C. Scott, G.J. Flesch, E.J. Moyer, J.W. Elkins, G.S. Dutton, D.F. Hurst, F.L. Moore, E.A. Ray, P.A. Romashkin, S.E. Strahan, J. Geophys. Res. 106 (2001) 32295–32314.
[7] G.P. Stiller, T. von Clarmann, M. Horfner, N. Glatthor, U. Grabowski, S. Kellmann, A. Kleinert, A. Linden, M. Milz, T. Reddmann, T. Steck, H. Fischer, B. Funke, M. Lopez-Puertas, A. Engel, Atmos. Chem. Phys. 8 (2008) 677–695.
[8] A.T. Brown, M.P. Chipperfield, C. Boone, C. Wilson, K.A. Walker, P.F. Bernath, J. Quant. Spectrosc. Radiat. Trans. 112 (2011) 2552.
[9] F.J. Haenel, G.P. Stiller, T. von Clarmann, B. Funke, E. Eckert, N. Glatthor, U. Grabowski, S. Kellmann, M. Kiefer, A. Linden, T. Reddmann, Atmos. Chem. Phys. 15 (2015) 13161–13176.
[10] C. Chapados, G. Birnbaum, J. Mol. Spectrosc. 15 (1988) 132–323.
[11] B. Bobin, C. Bordé, J. Bordé, C. Bréant, J. Mol. Spectrosc. 121 (1987) 91.
[12] O. Acef, C. Bordé, A. Clairon, G. Pierre, B. Sartakov, J. Mol. Spectrosc. 199 (2000) 188.
[13] V. Boudon, H. Bürger, E.B. M'Kami, J. Mol. Spectrosc. 205 (2001) 304.
[14] D. Bermejo, R.Z. Martinez, E. Loubignac, G. Pierre, J. Mol. Spectrosc. 201 (2000) 164.
[15] V. Boudon, D. Bermejo, J. Mol. Spectrosc. 213 (2002) 139.
[16] V. Boudon, J.L. Domenech, D. Bermejo, H. Willner, J. Mol. Spectrosc. 228 (2004) 392.
[17] V. Boudon, L. Manceron, F. Kwabia Tchana, M. Loëte, L. Lago, P. Roy, Phys. Chem. Chem. Phys. 16 (2014) 1415.
[18] C.P. Rinsland, A. Goldman, J.M. Flaud, J. Quant. Spectrosc. Radiat. Trans. 48 (5-6) (2004) 693.
[19] J.M. Flaud, C. Piccolo, B. Carli, A. Perrin, L.H. Coudert, J.L. Teffo, L.R. Brown, Atmos. Ocean. Opt. 16 (2003) 172–182.
[20] M. Faye, A. Leven, V. Boudon, L. Manceron, P. Asselin, F. Kwabia Tchana, P. Roy, Mol. Phys. 112 (2014) 909059.
[21] P. Varanasi, Z. Li, V. Nemchikov, A. Cherbini, J. Quant. specrosc. Radiat. Trans. 52 (3) (1994) 323.
[22] M. Faye, V. Boudon, M. Loëte, P. Roy, L. Manceron, J. Mol. Spectrosc. 325 (2016) 35–41.
[23] M. Faye, V. Boudon, M. Loëte, P. Roy, L. Manceron, J. Quant. Spectrosc. Radiat. Trans. 190 (2017) 38–47.
[24] P. Roy, J.B. Brubach, M. Rouziéres, O. Pirali, L. Manceron, F. Kwabia Tchana, Rev. Electricité et Electron. 2 (2008) 23.
[25] J.B. Brubach, L. Manceron, M. Rouziéres, O. Pirali, D. Balcon, F. Kwabia Tchana, V. Boudon, M. Tudorie, T. Huet, A. Cuisset, P. Roy, Infrared Phys. Technol. (2009) 112.
[26] F.K. Tchana, F. Willaert, X. Landsheere, J.-M. Flaud, L. Lago, M. Chapuis, P. Roy, L. Manceron, Rev. Sci. Inst. 84 (2013) 093101.
[27] M. Faye, M. Bordessoule, B. Kanouté, P. Roy, L. Manceron, Rev. Sci. Inst. 87 (2016) 063119.
[28] C. Wenger, V. Boudon, J.-P. Champion, G. Pierre, J. Quant. Spectrosc. Radiat. Trans. 66 (2000) 1.
[29] C. Wenger, V. Boudon, M. Rotger, M. Sanzharov, J.-P. Champion, J. Mol. Spectrosc. 251 (2008) 102.
[30] R. McDowell, B. Krohn, Spectrochim. Acta. 42A (1986) 371.
[31] J.P. Champion, M. Loëte, G. Pierre, in Spectroscopy of the Earth's Atmosphere and Interstellar Medium, in: K.N. Rao, A. Weber (Eds.), Academic Press, San Diego, 1992, pp. 339–422.
[32] V. Boudon, J.-P. Champion, T. Gabard, M. Loëte, F. Michelot, G. Pierre, M. Rotger, C. Wenger, M. Rey, J. Mol. Spectrosc. 228 (2004) 620–634.
[33] C. Chapados, G. Birnbaum, J. Mol. Spectrosc. 132 (1988) 323.
[34] R.K. Heenan, The molecular structures of BrF_5 and IF_5; and vibrational potentials for some spherical top molecules, edited by University of Reading. Thesis, 1979.
[35] K. Kim, R.S. McDowell, W.T. King, J. Chem. Phys. 73 (1980) 36.
[36] J.H. Van Vleck, Phys. Rev. 33 (1929) 467–506.